Coarse-grained single-particle dynamics in two-dimensional solids and liquids

Jörg R. Silbermann,[1,*] Martin Schoen,[1,†] and Sabine H. L. Klapp[1,2,‡]
[1]*Stranski-Laboratorium für Physikalische und Theoretische Chemie, Sekretariat C7, Technische Universität Berlin, Straße des 17, Juni 115, D-10623 Berlin, Germany*
[2]*Institut für Theoretische Physik, Sekretariat EW 7-1, Technische Universität Berlin, Hardenbergstraße 36, D-10623 Berlin, Germany*
(Received 18 March 2008; published 16 July 2008)

We consider the dynamics of a single tagged particle in a two-dimensional system governed by Lennard-Jones interactions. Previous work based on the Mori-Zwanzig projection operator formalism has shown that the single-particles dynamics can be described via a generalized Langevin equation (GLE) which is exact within the harmonic approximation, that is, for a low-temperature solid [J. M. Deutch and R. Silbey, Phys. Rev. A **3**, 2049 (1971)]. In the present work we explore to what an extent the GLE reproduces the effective dynamics under thermodynamic conditions where the harmonic approximation is no longer justified. To this end we compute characteristic time autocorrelation functions for the tagged particle in molecular dynamics simulations of the full system and compare these functions with those obtained from solving the GLE. At low temperatures we find excellent agreement between both data sets. Deviations emerge at higher temperatures which are, however, surprisingly small even in the high-temperature liquid phase.

DOI: 10.1103/PhysRevE.78.011201 PACS number(s): 61.20.Lc, 83.10.Mj

I. INTRODUCTION

There is increasing interest in understanding the dynamics of complex fluids such as colloidal suspensions, polymeric and surfactant solutions, or biomolecular systems. A common feature of such systems is that interesting and technologically or biologically important effects such as mesophase formation or protein folding occur on microsecond to second time scales. These are currently far out of reach for conventional molecular dynamics (MD) simulations involving all degrees of freedom characterizing the microscopic system. As a consequence, much effort is spent to develop coarse-grained ("mesoscopic") simulation techniques [1–3], all of which rely on a drastic reduction of variables. This procedure implies two steps. First one has to identify the relevant "slow" degrees of freedom and, in turn, the remaining fast ones which one usually wants to account for only in an average manner. Familiar examples of slow variables (whose choice depends, of course, on the phenomenon of interest) are the positions and momenta of heavy colloidal particles in a solvent, or the center of masses and conjugated momenta of the building blocks of a polymer chain. The second main step consists of setting up a suitable coarse-grained equation of motion for these slow degrees of freedom. Various mesoscopic simulation methods such as Brownian dynamics and dissipative particle dynamics [4,5] make an ansatz for the effective dynamics. Typically, the total force acting on a slow particle separates into conservative contributions (which are gradients of an effective interaction potential) and nonconservative contributions mimicking the influence of the neglected degrees of freedom. These nonconservative parts are often formulated to optimize the computation, especially when ones focusses on static equilibrium properties (for which the precise shape of the nonconservative forces should be irrelevant). For dynamic applications such as simulations of hydrodynamic "swimmers," shear thickening or thinning, or conformational dynamics in biomolecules, however, it would desirable if these nonconservative contributions could be derived from the microscopic system. Indeed, the conservative contributions to the effective force can be rigorously defined on the basis of the partition sum related to the microscopic Hamiltonian [6–8]. The role of the resulting effective interactions for the dynamic properties of fluid mixtures is discussed in Ref. [9].

A systematic way to obtain coarse-grained equations of motion was proposed by Mori [10] and Zwanzig [11] who developed the projection operator formalism in the 1960's. The main idea consists of introducing a projection operator into the (typically Hamiltonian) dynamics of the microscopic system, that serves to average over the irrelevant degrees of freedom. This procedure leads to an exact generalized Langevin equation (GLE) for the slow variables to which we shall refer as "particles" henceforth. Apart from conservative forces the GLE involves a dissipative force reflecting the fact that the motion of slow particles is retarded by friction from the fast ones, and the so-called random force arising from collisions of the fast and slow particles. For practical applications, the main drawback of the GLE method is that it is generally unclear how to actually calculate the random force. The same is consequently true for the dissipative contribution which is related to the random part through the fluctuation-dissipation theorem (see, e.g., Ref. [12]). Thus, simplifications have to been done, the simplest one being the Markov approximation leading to the conventional Langevin equation (characterized by a δ-like friction kernel) [12]. More sophisticated approximations have been recently proposed in projection-operator investigations of polymer dynamics [13], protein folding [14,15], and various "multiscale" model systems [16–18].

Interestingly, there exists one particular system for which the random force appearing in the GLE can be calculated in an exact manner. This is a harmonic lattice consisting of one

*joerg.silbermann@fluids.tu-berlin.de
†martin.schoen@fluids.tu-berlin.de
‡sabine.klapp@fluids.tu-berlin.de

or more colloidal (tagged) particles in a "bath" of (usually much lighter) particles. The corresponding rigorous expressions for the random forces have been first derived by Deutch and Silbey [19] and later, in a slightly generalized manner, by Wada and Hori [20]. Clearly, the harmonic lattice is a special system, which has, nevertheless, relevance for a variety of polymeric systems such as physical gels [21] and unentangled polymer melts (see Ref. [22], and references therein). Moreover, one-dimensional harmonic models have recently been investigated to study the consequences of basic coarse-graining concepts such as grouping of particles into clusters [17,23,24].

From a more physical point of view, harmonic lattices are important if one thinks of colloidal solutions in the low-temperature solid state [25]. Having this in mind, our goal in the present paper is to explore to what an extent the exact GLE of the harmonic system reproduces the effective dynamics of a single particle under thermodynamic conditions where the harmonic approximation is no longer justified. Specifically, we consider a two-dimensional model system of spherical particles in the solid and the liquid phase. To benchmark the performance of the GLE (that is, the exact prescription of the random forces) we compute characteristic time autocorrelation functions for the tagged particle in MD simulations of the full system and compare these functions with those obtained by solving the GLE. Our results reveal a surprisingly wide applicability of the effective equation of motion. Indeed, the GLE turns out to generate accurate results even in high-temperature solids and (dense) liquids.

The remainder of this paper is organized as follows. In Sec. II we describe the theoretical background of our study, including the main steps in deriving the GLE on which our results are based. The two-dimensional model system used in the actual simulations is introduced in Sec. III. Our numerical results will be discussed in Sec. IV, followed by concluding remarks in Sec. V.

II. THEORETICAL BACKGROUND

Following Deutch and Silbey [19] we consider a system composed of $N+1$ particles without internal degrees of freedom. Among these particles, one (the "tagged" particle) has mass m_0, and we characterize its position and momentum by vectors $\mathbf{r}_0$ and $\mathbf{p}_0$, respectively. The other particles (forming the "bath") have mass m and are characterized by vectors $\mathbf{r}_i$ and $\mathbf{p}_i$, $i=1,\ldots,N$. The total Hamiltonian of the system is given as

$$H = H' + \frac{\mathbf{p}_0^2}{2m_0} = \sum_{i=1}^{N} \frac{\mathbf{p}_i^2}{2m} + U(\mathbf{r}_0, \mathbf{r}^N) + \frac{\mathbf{p}_0^2}{2m_0}, \tag{2.1}$$

where $U(\mathbf{r}_0, \mathbf{r}^N)$ is the total potential energy which depends on the spatial configuration $\mathbf{r}^N=\mathbf{r}_1,\ldots,\mathbf{r}_N$ of the bath particles and of the position $\mathbf{r}_0$ of the tagged particle. Thus, the Hamiltonian H' introduced in Eq. (2.1) defines a modified system in which the tagged particle interacts with the others but has, at the same time, zero kinetic energy. In other words, in the modified system the tagged particle is positionally fixed (in fact, it rather acts as an external potential on the bath particles). We shall refer to the system described by H' as the "reference system."

Consider now the force $\mathbf{F}_0(t)=\dot{\mathbf{p}}_0(t)=\partial\mathbf{p}_0(t)/\partial t$ acting on the tagged particle at time t in the original system where all $N+1$ particles can move. Its spatio-temporal evolution is governed by the Liouville operator $\mathcal{L}$

$$i\mathcal{L} = \sum_{i=0}^{N} \left(\frac{\mathbf{p}_i}{m_i} \frac{\partial}{\partial \mathbf{r}_i} + \mathbf{F}_i \frac{\partial}{\partial \mathbf{p}_i} \right), \tag{2.2}$$

where $m_1=\cdots=m_N=m$. We can relate $\mathbf{F}_0(t)$ to the corresponding force at $t=0$ via the propagator $\exp(i\mathcal{L}t)$, that is

$$\mathbf{F}_0(t) = \exp(i\mathcal{L}t)\mathbf{F}_0(0). \tag{2.3}$$

Equation (2.3) corresponds to the integrated form of the general Liouville equation $\dot{A}(t)=i\mathcal{L}A(t)$ for a dynamic variable A, specialized to the case where $\mathcal{L}$ is not explicitly time dependent.

The goal is now to derive an effective, i.e., coarse-grained equation for $\mathbf{F}_0(t)$ where the bath particles' coordinates and forces do not appear explicitly anymore. To this end we split the Liouville operator into two contributions [19]

$$i\mathcal{L} = i\mathcal{L}^{(0)} + i\mathcal{L}^{(B)}, \tag{2.4}$$

where

$$i\mathcal{L}^{(0)} = \frac{\mathbf{p}_0}{m_0} \cdot \frac{\partial}{\partial \mathbf{r}_0} + \mathbf{F}_0 \cdot \frac{\partial}{\partial \mathbf{p}_0}, \tag{2.5a}$$

$$i\mathcal{L}^{(B)} = \sum_{j=1}^{N} \left(\frac{\mathbf{p}_j}{m} \cdot \frac{\partial}{\partial \mathbf{r}_j} + \mathbf{F}_j \cdot \frac{\partial}{\partial \mathbf{p}_j} \right). \tag{2.5b}$$

From the above definitions it is clear that $\mathcal{L}^{(0)}$ and $\mathcal{L}^{(B)}$ act on the tagged particle and on the bath, respectively. Moreover, as shown in Appendix A 1, the operators $\mathcal{L}$, $\mathcal{L}^{(B)}$, and $\mathcal{L}^{(0)}$ satisfy the integral equation

$$\exp(i\mathcal{L}t) = \exp(i\mathcal{L}^{(B)}t) + \int_0^t dt' \exp[i\mathcal{L}(t-t')] \times i\mathcal{L}^{(0)} \exp(i\mathcal{L}^{(B)}t'). \tag{2.6}$$

We can now employ Eq. (2.6) to rewrite the equation of motion for $\mathbf{F}_0(t)$ given in Eq. (2.3). Introducing the projection operator $\mathcal{P}$ we may write

$$i\mathcal{L}^{(0)} = \mathcal{P}i\mathcal{L}, \tag{2.7a}$$

$$i\mathcal{L}^{(B)} = (\mathcal{I}-\mathcal{P})i\mathcal{L}, \tag{2.7b}$$

where we have also introduced the unit operator $\mathcal{I}$. Combining Eqs. (2.3), (2.5), and (2.7) we obtain

$$\mathbf{F}_0(t) = \mathbf{F}_0^+(t) + \int_0^t dt' \exp[i\mathcal{L}(t-t')] i\mathcal{P}\mathcal{L}\mathbf{F}_0^+(t'). \tag{2.8}$$

In Eq. (2.8), the quantity $\mathbf{F}_0^+(t)$ is defined as

$$\mathbf{F}_0^+(t) \equiv \exp[i(\mathcal{I}-\mathcal{P})\mathcal{L}t]\mathbf{F}_0(0) = \exp(i\mathcal{L}^{(B)}t)\mathbf{F}_0(0). \tag{2.9}$$

From Eq. (2.9) it follows that $\mathbf{F}_0^+(0)=\mathbf{F}_0(0)$. For all later times ($t>0$) $\mathbf{F}_0^+(t)$ is often called the "random force."

A more explicit form of the time integral appearing in Eq. (2.8) can be obtained by specifying the projection operator $\mathcal{P}$. One possible choice suggested by Deutch and Silbey [19] reads

$$\mathcal{P}(\cdots) \equiv \langle\cdots\rangle = \frac{1}{Q'(\mathbf{r}_0)}\prod_{i=1}^{N}\int d\mathbf{p}_i \int d\mathbf{r}_i \cdots \exp(-\beta H'), \tag{2.10}$$

where $\beta=1/k_BT$ (with k_B and T being Boltzmann's constant and temperature, respectively) and $Q'(\mathbf{r}_0)=\Pi_{i=1}^{N}\int d\mathbf{p}_i\int d\mathbf{r}_i \exp(-\beta H')$. Thus, the action of $\mathcal{P}$ corresponds to "integrating out" the positions and momenta of the bath particles, which are considered as irrelevant ("fast") degrees of freedom. More precisely, an application of $\mathcal{P}$ corresponds to averaging in an equilibrium statistical (canonical) ensemble governed by the Hamiltonian of the "reference system" introduced in Eq. (2.1) (this definition of $\mathcal{P}$ differs from the more common Mori-Zwanzig definition [10] where one averages canonically over all degrees of freedom including those of the tagged particle). Note that, within the present definitions, the partition sum $Q'(\mathbf{r}_0)$ still depends on the position of the tagged particle since the integrations are carried out only over the positions and momenta of the bath particles.

From the above definition of $\mathcal{P}$ it follows (see Appendix A 2) that the last term in the integrand appearing in Eq. (2.8) can be rewritten according to

$$i\mathcal{P}\mathcal{L}\mathbf{F}_0^+(t) = i\mathcal{P}\mathcal{L}^{(0)}\mathbf{F}_0^+(t) = \left(\frac{\partial}{\partial\mathbf{p}_0} - \frac{\beta\mathbf{p}_0}{m_0}\right)\langle\mathbf{F}_0^+(0)\cdot\mathbf{F}_0^+(t)\rangle. \tag{2.11}$$

Inserting Eq. (2.11) into Eq. (2.8) we obtain

$$\mathbf{F}_0(t) = \mathbf{F}_0^+(t) + \int_0^t dt' \exp[i\mathcal{L}(t-t')] \times\left(\frac{\partial}{\partial\mathbf{p}_0} - \frac{\beta\mathbf{p}_0}{m_0}\right)\langle\mathbf{F}_0^+(0)\cdot\mathbf{F}_0^+(t')\rangle. \tag{2.12}$$

Equation (2.12) is exact, irrespective of the details of the total potential energy. However, for general interactions one does not know how to compute (or measure) the "random" force $\mathbf{F}_0^+(t)$. In particular, $\mathbf{F}_0^+(t)$ cannot be derived from an interaction potential unlike $\mathbf{F}_0(t)=\dot{\mathbf{p}}_0(t)=-(\partial U/\partial\mathbf{r}_0)(t)$.

A remarkable exception is the special case of a harmonic crystal, where the potential energy is a quadratic form of the positions. This case has been studied by Deutsch and Silbey [19] who demonstrated that the random force $\mathbf{F}_0^+(t)$ is identical to the total force $\mathbf{F}_0^{\mathrm{ref}}(t)$ acting on the same (tagged) particle in the corresponding "reference system." We recall [see text after Eq. (2.1)] that the reference system is characterized by a spatially fixed tagged particle, with the remaining bath particles moving under the influence of their mutual interactions and their interaction with the fixed tagged particle. The force of interest can then simply be calculated as a "mechanical" force, that is,

$$\mathbf{F}_0^+(t) = \mathbf{F}_0^{\mathrm{ref}}(t) = \sum_{i=1}^{N}\mathbf{F}_{0i}(t) = -\sum_{i=1}^{N}\frac{\partial U}{\partial\mathbf{r}_{0i}}, \tag{2.13}$$

where the right side of Eq. (2.13) involves the pair forces $\mathbf{F}_{0i}(t)$ between a bath particle and the fixed one ($\mathbf{r}_{0i}=\mathbf{r}_0-\mathbf{r}_i$ is the corresponding separation vector). Clearly, these pair forces are easily accessible in a conventional computer simulation. From a physical point of view, positional fixation of the tagged particle can be achieved by assigning an infinite mass $m_0\to\infty$ to it (in the reference system). Therefore, we use the notation $\mathbf{F}_0^{(\infty)}(t)$ instead of $\mathbf{F}_0^{\mathrm{ref}}(t)$ from now on.

The equivalence of $\mathbf{F}_0^+(t)$ and $\mathbf{F}_0^{(\infty)}(t)$ [see Eq. (2.13)] for harmonic crystals leads to a significant simplification of the integrand appearing on the right side of the equation of motion (2.12). First, since $\mathbf{F}_0^{(\infty)}(t)$ is conservative (and, thus, independent of $\mathbf{p}_0$), the derivative of the autocorrelation function $\langle\mathbf{F}_0^{(\infty)}(0)\cdot\mathbf{F}_0^{(\infty)}(t)\rangle$ with respect to $\mathbf{p}_0$ vanishes. Secondly, because we are focussing on systems at thermodynamic equilibrium, the autocorrelation function is stationary (i.e., independent of the time origin), that is,

$$\exp[i\mathcal{L}(t-t')]\langle\mathbf{F}_0^{(\infty)}(0)\cdot\mathbf{F}_0^{(\infty)}(t')\rangle = \langle\mathbf{F}_0^{(\infty)}(t-t')\cdot\mathbf{F}_0^{(\infty)}(t)\rangle \overset{t\to t'}{=} \langle\mathbf{F}_0^{(\infty)}\cdot\mathbf{F}_0^{(\infty)}(t')\rangle. \tag{2.14}$$

Using these properties we rewrite Eq. (2.12) as a generalized Langevin equation (GLE) [19]

$$\mathbf{F}_0(t) = \mathbf{F}_0^{(\infty)}(t) - \frac{\beta}{m_0}\int_0^t dt'\,\mathbf{p}_0(t-t')\langle\mathbf{F}_0^{(\infty)}(0)\cdot\mathbf{F}_0^{(\infty)}(t')\rangle. \tag{2.15}$$

Notice that Eq. (2.15) is exact within the harmonic approximation for the potential energy. We also note that its validity does not depend on the mass ratio m_0/m in the original system.

A generalization of Eq. (2.15) was derived by Wada and Hori [20]. Considering again harmonic crystals, and using a slightly different definition of the partial Liouville operators $\mathcal{L}^{(0)}$ and $\mathcal{L}^{(B)}$ [see Eq. (2.5)] they showed that the mass of the tagged particle in the reference system can be set to an arbitrary value M. As a consequence, the tagged particle in the reference system may move (assuming that M is finite). The total force acting on this particle, which we denote by $\mathbf{F}_0^{(M)}(t)$, can then again be calculated as a mechanical force given by Eq. (2.13). In this case, the generalized GLE can be written as [20]

$$\mathbf{F}_0(t) = \mathbf{F}_0^{(M)}(t) - \beta\left(\frac{1}{m_0}-\frac{1}{M}\right) \times\int_0^t dt'\,\mathbf{p}_0(t-t')\langle\mathbf{F}_0^{(M)}(0)\cdot\mathbf{F}_0^{(M)}(t')\rangle. \tag{2.16}$$

By construction, Eq. (2.16) reduces to the Deutch-Silbey form [see Eq. (2.15)] in the limit $M\to\infty$ (corresponding to a

spatially fixed tagged particle in the reference system). On the other hand, in the special case $M=m_0$ the second term on the right side of Eq. (2.16) vanishes altogether. This is reasonable, because $M=m_0$ implies equivalence between the original and the reference system, and thus $\dot{\mathbf{p}}_0(t)\equiv\mathbf{F}_0(t)=\mathbf{F}_0^{(m_0)}(t)$ irrespective of the specific form of the interactions.

III. MODEL AND STRATEGY OF INVESTIGATION

Based on the GLE (2.16) derived in the preceding Sec. II the effective dynamics of a given particle immersed in a bath (solvent) can be computed in an exact fashion. We recall, however, that this equation of motion relies on a particular shape of the total potential energy, that is, the harmonic approximation. For a realistic system of atoms or colloidal particles one expects this approximation to be justified within the low-temperature solid phase, that is, when the deviations of the actual particle positions from their lattice sites are so small that anharmonic terms in an expansion of the true potential energy can be neglected. Our main objective in the present work is to explore to what an extent the GLE is capable of (approximately) reproducing the dynamics under conditions where the harmonic approximation is no longer justified. That is, we are specifically interested in high-temperature solids and the liquid phase.

To this end we consider a simple model system of spherical particles confined to a plane, which we investigate via molecular dynamics (MD) simulations (for technical details, see Appendix B). Choosing a two-dimensional (2D) model system rather than a 3D one significantly restricts the computational burden of our numerical investigations. Indeed, already for our 2D systems we have found that long simulations involving up to 10^8 time steps combined with relatively large systems (particle numbers $N\sim 3000-6000$) are required to obtain acceptable statistics. Extending these system sizes into the third spatial dimension would correspond to an enormous additional computational effort. Moreover, 2D systems are interesting themselves since their physical behavior can be markedly different from that of typical 3D systems. An example is the crystallization and melting of 2D colloidal systems recently observed in experiments [26,27]. Given that both solid and fluid phases were found in such systems, it seems particularly interesting to explore the validity of the GLE under anharmonic conditions.

Our 2D model system consists of $N+1$ particles interacting via a shifted and truncated Lennard-Jones (LJ) potential, that is,

$$u(r)=\begin{cases} u_{\mathrm{LJ}}(r)-u_{\mathrm{LJ}}(r_c)-u'_{\mathrm{LJ}}(r_c)(r-r_c), & r\leqslant r_c,\\ 0, & r>r_c, \end{cases} \tag{3.1}$$

where r is the distance between a pair of particles, $u'=du/dr$, and r_c is a cutoff distance, at which both the potential u and its first derivative (and thus, the corresponding force) vanish. The actual LJ potential appearing in Eq. (3.1) is given by

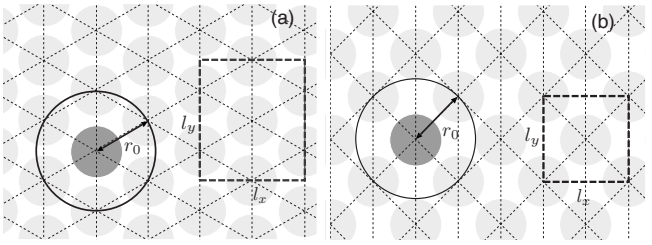

FIG. 1. Sketch of a particle on a hexagonal (a) and quadratic (b) lattice with nearest-neighbor distance r_0. Dashed rectangles with side lengths $l_x=l_y=\sqrt{2}r_0$ (square lattice) or, respectively, $l_x=\sqrt{3}r_0$, $l_y=2r_0$ (hexagonal lattice) indicate subunits of the simulation cell.

$$u_{\mathrm{LJ}}(r)=4\varepsilon\left[\left(\frac{\sigma}{r}\right)^{12}-\left(\frac{\sigma}{r}\right)^{6}\right]. \tag{3.2}$$

For simplicity we consider a monodisperse system where the diameter σ of the tagged particle is equal to that of the bath particles. We further specialize to the case $m_0=m$, that is, the tagged particles has the same mass as the bath particles (note that this choice concerns the original system but not the reference system, where the mass M of the tagged particles is different from m).

At low temperatures and high densities the particles arrange into a solidlike state with long-range planar positional order. In the present work we consider two different 2D lattice structures which are illustrated in Fig. 1. The hexagonal lattice [see Fig. 1(a)], where each particle has six nearest neighbors, corresponds to the thermodynamically stable crystal structure for a variety of systems such as LJ particles [28], hard disks [29], and repulsive paramagnetic colloids [25–27]. The quadratic lattice [see Fig. 1(b)], where each particle has four nearest neighbors, is more "open" than the hexagonal one. For the systems mentioned above the quadratic lattice is only metastable even at very low temperatures. A rather "exotic" exception is a granular crystal modeled with an embedded-atom potential. This system does indeed exhibit a stable solid phase with quadratic lattice structure [30]. We have included the quadratic structure in our investigations of the 2D LJ systems to explore the influence of lattice geometry, particularly the role of the number of neighbors.

To define the densities of the solid states we set the nearest-neighbor separation r_0 equal to the distance where the truncated LJ potential [see Eq. (3.1)] has its minimum, that is

$$\left.\frac{du(r)}{dr}\right|_{r_0}\overset{!}{=}0, \tag{3.3}$$

which yields $r_0\simeq 1.1384\sigma$ for the present choice $r_c=1.6\sigma$ (this choice for r_c corresponds to a LJ system with a very short-ranged attraction, that is, a nearest-neighbor attraction in the solid phase). The corresponding dimensionless number densities are $\rho^*\equiv\rho\sigma^2=(\sigma/r_0)^2 2/\sqrt{3}\approx 0.891$ for the hexagonal lattice and $\rho^*=(\sigma/r_0)^2\simeq 0.772$ for the quadratic lattice, respectively (with $\rho=N/A$, A being the area of the cell).

Based on the 2D model described above our investigation of the performance of the GLE proceeds as follows.

(1) We first determine the dynamics of the tagged particle of mass m_0 in the original system governed by the full Hamiltonian H [see Eq. (2.1)]. This is done by means of MD simulations at fixed density and temperature. As explained in Appendix B we control the temperature implicitly via stochastic boundary conditions. By using sufficiently large systems we can ensure that this technical procedure does not influence the dynamical properties of interest. Our target quantities are the (non-normalized) velocity-autocorrelation function (VACF) of the tagged particle

$$\Psi_{vv}(t) = \langle \mathbf{v}_0(\tilde{t}) \cdot \mathbf{v}_0(\tilde{t}+t) \rangle \tag{3.4}$$

and the force-autocorrelation function (FACF)

$$\Psi_{\mathrm{ff}}(t) = \langle \mathbf{F}_0(\tilde{t}) \cdot \mathbf{F}_0(\tilde{t}+t) \rangle. \tag{3.5}$$

In Eqs. (3.4) and (3.5), $\langle \cdots \rangle$ denotes an average over time origins $\tilde{t}$. The FACF plays a key role since it is the force $\mathbf{F}_0(t)$ which is described by the GLE [see Eq. (2.16)]. In fact, the only reason not to consider $\mathbf{F}_0(t)$ directly is that its time average vanishes, thus making a numerical investigation impossible. Therefore, the FACF is the quantity where one would expect a failure of the GLE to become visible most clearly.

(2) Parallel to the MD simulations of the original system we perform MD simulations of the corresponding (Wada-Hori) reference system, defined by changing the mass of the tagged particle from m_0 to M. Apart from this difference the two systems are identical, including their thermodynamic state characterized by temperature and density. In particular, when the original system is a liquid the reference system is a liquid as well. For given M we then compute the force $\mathbf{F}_0^{(M)}(t)$ and its autocorrelation function

$$\Phi^{(M)}(t) = \langle \mathbf{F}_0^{(M)}(\tilde{t}) \cdot \mathbf{F}_0^{(M)}(\tilde{t}+t) \rangle. \tag{3.6}$$

(3) Based on $\mathbf{F}_0^{(M)}(t)$ and $\Phi^{(M)}(t)$ we calculate the effective force $\mathbf{F}_0(t)$ by numerical solution of the GLE (2.16). We then use this reproduced force to compute the trajectory of the tagged particle according to the coarse-grained dynamics, and, based on that, the reproduced versions of the time-autocorrelation functions specified in Eqs. (3.4) and (3.5). These functions will be denoted (for a specific value of M) by $\Psi_{vv}^{(M)}(t)$ and $\Psi_{ff}^{(M)}(t)$. Comparing the latter functions with the original time autocorrelation functions we can finally benchmark the performance of the GLE.

IV. NUMERICAL RESULTS

Our subsequent discussion of the effective dynamics proceeds as follows. We start in Sec. IV A by considering lattice systems with hexagonal or quadratic positional structure, focussing on very low temperatures. Under these conditions we expect the harmonic approximation (which is the prerequisite for the validity of the GLE) to work best. In Sec. IV A we also discuss, from a practical point of view, possible choices for the dimensionless mass $M^*=M/m_0$ characterizing the tagged particle in the reference system. The subsequent Sec. IV B deals with temperatures around the melting point, where we restrict our analysis of solid states to the hexagonal lattice. Indeed, for the density considered it turned out that the quadratic lattice is (meta)stable only up to a temperature $T^* \simeq 10^{-4}$ (with $T^*=k_BT/\varepsilon$ being the dimensionless temperature). At higher temperatures, the system (when started from a quadratic lattice) quickly collapses into an inhomogeneous mixture of hexagonal and gaslike regions, indicating global instability of the squarelike order. Section IV B also includes results for the dense liquid ($\rho^*=0.891$) into which the hexagonal solid melts upon increase of T^*. Finally, to illustrate the influence of density we present in Sec. IV C some liquid-state results obtained at $\rho^*=0.6$.

A. Effective dynamics in low-temperature solid states

In this section we consider the dynamics of the tagged particle at $T^*=10^{-5}$. This value is representative for the temperature range where the harmonic approximation of the total potential energy $U(\mathbf{r}_0,\mathbf{r}^N)$ is justified. We have explicitly checked this point by comparing averages for the potential energy and the velocity autocorrelation function $\langle \mathbf{v}_0(t) \cdot \mathbf{v}_0(0) \rangle$ in the harmonic system, on one hand, and the full system, on the other hand. At $T^*=10^{-5}$ these functions turned out to be indistinguishable.

Given the validity of the harmonic approximation for $U(\mathbf{r}_0,\mathbf{r}^N)$ we would expect the GLE to reproduce the tagged particle's dynamics exactly (see Sec. II). As explained in Sec. III we can test the GLE by comparing the velocity autocorrelation function $\Psi_{vv}(t)$ of the tagged particle in the fully interacting system [see Eq. (3.4)] with the function $\Psi_{vv}^{(M)}(t)$ obtained by solving the GLE (using the input from a reference system characterized by a mass M).

Results for the dimensionless functions $\Psi_{vv}(t)$ and $\Psi_{vv}^{(M)}(t)$ are shown in Fig. 2 where we consider both the hexagonal and the quadratic lattice. For both structures the reference system was characterized by $M^*=\infty$, corresponding to the original Deutch-Silbey approach [19] where the position of the tagged particle in the reference system is fixed. Inspecting the data in Fig. 2(a) one sees that $\Psi_{vv}^{(M)}(t)$ indeed coincides with $\Psi_{vv}(t)$ for the quadratic lattice, thus satisfying the relations formulated by Deutch and Silbey [19]. For the hexagonal lattice, however, the data in Fig. 2(b) reveal strong deviations between $\Psi_{vv}(t)$ and $\Psi_{vv}^{(M)}(t)$.

In order to shed some light on the specific role of the hexagonal lattice we computed the memory functions $K(t)$ of $\Psi_{vv}(t)$ for both lattice types. The function $K(t)$ is defined through the Volterra equation [31] (for the numerical solution, see Ref. [32])

$$\frac{d}{dt}\Psi_{vv}(t) = -\int_0^t dt' \Psi_{vv}(t-t')K(t'). \tag{4.1}$$

From Eq. (4.1) it is seen that $K(t)$ acts as a weighting function measuring to what an extent the VACF (more precisely, its time derivative) at a given time t is influenced by earlier times $t' < t$. Numerical results for the memory functions corresponding to the VACFs plotted in Fig. 2 are presented in Fig. 3. Comparing the data for the two lattice structures we

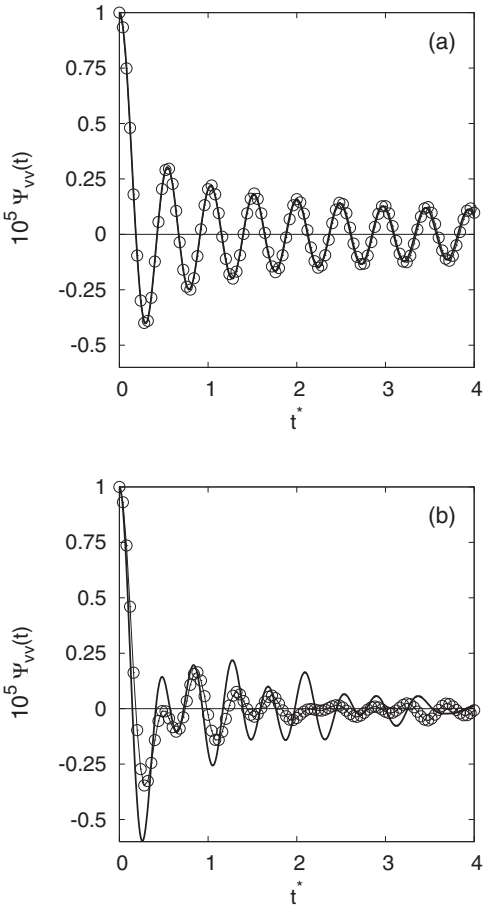

FIG. 2. The autocorrelation functions $\Psi_{vv}(t)$ (solid lines) and $\Psi_{vv}^{(M)}(t)$ obtained with $M^*=\infty$ (open circles) of the tagged particle in the quadratic (a) and hexagonal (b) lattice at $T^*=10^{-5}$.

observe, in both cases, an oscillatory behavior at short times whereas the long-time behavior and the overall magnitude of $K(t)$ differs markedly. In particular, the memory function corresponding to the quadratic lattice decays rather rapidly. On the other hand, for the hexagonal lattice $K(t)$ approaches a finite value as t becomes large, signaling an extremely long

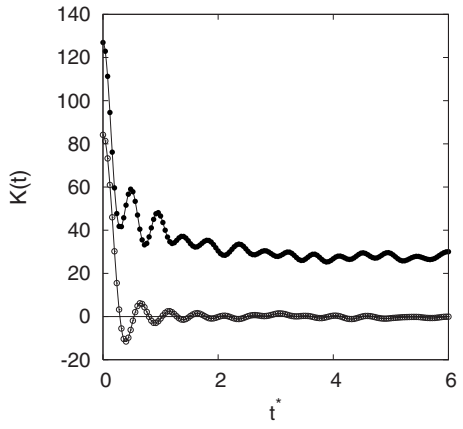

FIG. 3. The memory kernels $K(t)$ corresponding to the functions $\Psi_{vv}(t)$ plotted in Fig. 2 for the hexagonal (upper curve) and the quadratic (lower curve) lattice at $T^*=10^{-5}$.

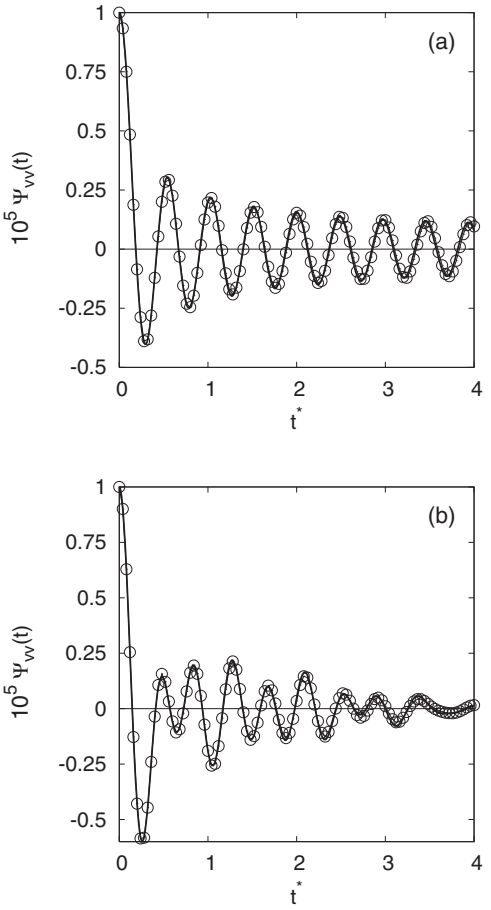

FIG. 4. The functions $\Psi_{vv}(t)$ (solid lines) and $\Psi_{vv}^{(M)}(t)$ (open circles) with $M^*=4$ for the quadratic (a) and the hexagonal (b) lattice at $T^*=10^{-5}$.

lifetime of the tagged particle's VACF at least on the time scale of our simulations.

As we will see below the same long lifetime characterizes the kernel of the GLE when $M^*=\infty$. This might explain why it is so difficult from a numerical point of view to reproduce the VACF (and likewise the corresponding FACF) according to the Deutch-Silbey GLE [see Eq. (2.15)] even under conditions where the harmonic approximation is justified.

Fortunately, this problem essentially disappears when we employ a reference system in the spirit of Wada and Hori [20] where the tagged particle can move (that is, the mass M has a finite value). In Fig. 4 we present numerical data for the VACF in its original and its reproduced form obtained with $M^*=4$. It is seen that the GLE now yields quasiexact results not only for the quadratic, but also for the hexagonal lattice. Thus, allowing the probe particle to move (i.e., choosing a sufficiently small value of M^*) strongly facilitates the numerical investigations as compared to the case $M^*\to\infty$.

We can understand this phenomenon by inspecting in more detail the influence of M^* on the kernel appearing in the GLE (2.16), that is, the force autocorrelation functions $\Phi^{(M)}(t)$ in the reference system defined in Eq. (3.6). It proves instructive to consider in parallel the power spectrum of $\Phi^{(M)}(t)$ defined as

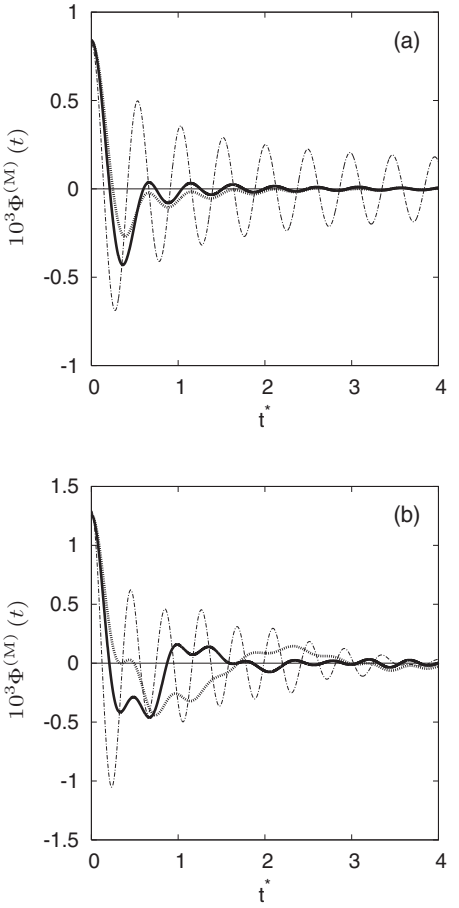

FIG. 5. The force autocorrelation function in the reference system $\Phi^{(M)}(t)$ for $M^*=4$ (solid line) and $M^*=10$ (dashed bold line) in the quadratic (a) and the hexagonal (b) lattice at $T^*=10^{-5}$. Included are data for the case $M^*=1$ corresponding to the original system (dash-dotted line).

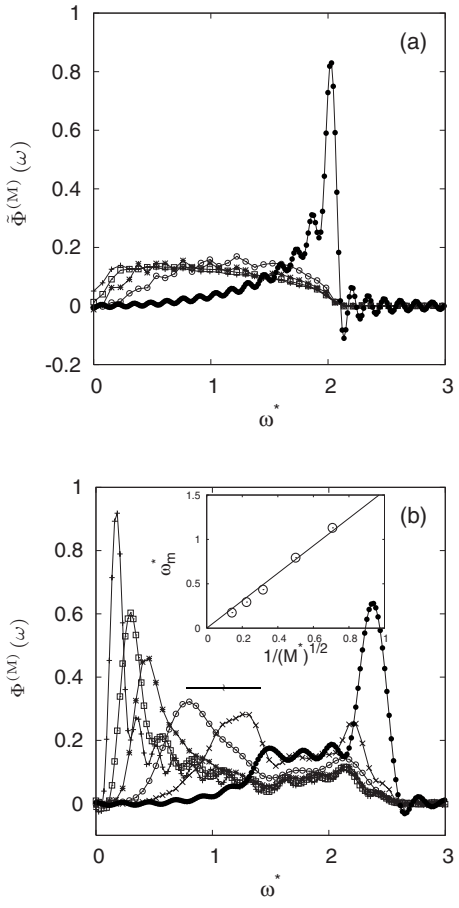

FIG. 6. Frequency spectra $\tilde{\Phi}^{(M)}(\omega)$ [see Eq. (4.2)] for the quadratic (a) and the hexagonal (b) lattice ($T^*=10^{-5}$), as obtained with $M^*=1$ (●), $M^*=2$ (×), $M^*=4$ (○), $M^*=10$ (∗), $M^*=20$ (□), and $M^*=50$ (+). The reduced frequency is defined as $\omega^*=\omega\sqrt{m\sigma^2/\varepsilon}$. The inset in (b) shows the dependence of the location of the main peak ω_m^* of $\tilde{\Phi}^{(M)}(\omega)$ on the mass M^*.

$$\tilde{\Phi}^{(M)}(\omega)=\int_0^\infty dt\Phi^{(M)}(t)\cos(\omega t). \tag{4.2}$$

Some exemplary data for $\Phi^{(M)}(t)$ and $\tilde{\Phi}^{(M)}(\omega)$ are plotted in Figs. 5 and 6, respectively, where we have included the case $M^*=1$ corresponding to the original system. At the low temperatures considered the latter represents essentially a system of harmonic oscillators which are coupled to each other via (nearest neighbor) LJ interactions. Neglecting these interactions for a moment one is left with a decoupled system of harmonic oscillators, in which the force autocorrelation function of the tagged particle can be evaluated analytically. Indeed, consider a single oscillator characterized by mass M and spring constant κ. Its momentum is given by $\mathbf{p}(t)=\sqrt{2Mk_BT}\hat{\mathbf{p}}\cos(\omega_{\mathrm{id}}t)$ where we have used the equipartition theorem in 2D for the initial value, and the frequency $\omega_{\mathrm{id}}=\sqrt{\kappa/M}$. The corresponding force autocorrelation function for given time origin t_0 then becomes $\mathbf{F}(t_0)\cdot\mathbf{F}(t+t_0)=2\kappa k_BT\sin(\omega_{\mathrm{id}}t_0)\sin[\omega_{\mathrm{id}}(t+t_0)]$. Finally, averaging over time origins in the interval $0\leqslant t_0\omega_{\mathrm{id}}\leqslant 2\pi$ yields $\Phi_{\mathrm{id}}^{(M)}(t)=(\kappa k_BT)\cos\omega_{\mathrm{id}}t$. The resulting frequency spectrum (in the positive frequency domain) is characterized by a single δ peak at ω_{id}. As seen from the data plotted in Figs. 5 and 6, the present interacting system ($M^*=1$) does have similarities with its ideal counterpart, as reflected in particular by the pronounced, single peak in $\tilde{\Phi}^{(M)}(\omega)$ (see Fig. 6). Deviations from the ideal case manifest themselves mainly as a damping of the oscillations in $\Phi^{(M)}(t)$ and a corresponding broader (nonsingular) distribution in $\tilde{\Phi}^{(M)}(\omega)$. We note in passing that these interaction effects seem to be more pronounced in the hexagonal case as reflected by the much faster damping of $\Phi^{(M)}(t)$ as compared to the quadratic case. This may be due to the fact that the number of nearest neighbors, and thus, the number of interaction partners is larger in the hexagonal lattice.

Further pronounced differences between the dynamics in the two lattices appear when the mass M^* of the tagged particle in the reference system is increased from one. Specifically, for the hexagonal system slow oscillations in $\Phi^{(M)}(t)$ emerge which extend to very long times. This is even more evident in the frequency domain [see Fig. 6(b)], where we see that the ("quasi-ideal") peak characterizing the spectrum at $M^*=1$ remains upon increasing M^*, but becomes strongly reduced in intensity. At the same time a second peak

develops (at a frequency ω_m) which increases in intensity and moves towards smaller and smaller frequencies upon increasing M^*. In fact, as demonstrated in the inset of Fig. 6(b), the position of the main peak of $\tilde{\Phi}(\omega)$ follows essentially the power law $\omega_m \sim M^{-1/2}$ characterizing an ideal noninteracting oscillator of mass M. Moreover, already for $M^* \approx 10$ this low-frequency peak dominates the spectrum. Therefore, and because the small-frequency behavior of $\tilde{\Phi}(\omega)$ determines that of $\Phi^{(M)}(t)$ at long times t [see Eq. (4.2)], it is clear that numerical calculations of $\Phi^{(M)}(t)$ in the reference system become increasingly difficult and time consuming. Moreover, the long lifetime of the force correlations, which act as a kernel in the GLE [see Eq. (2.16)], also implies that it becomes more and more difficult to evaluate the integral in the GLE accurately. In the quadratic lattice [see Fig. 6(a)], on the other hand, the frequency spectrum of the force autocorrelation function depends much less on M^*. In particular, there is no dominant low-frequency peak even at the largest values of M^* considered, as reflected by the fast decay of the corresponding time-dependent functions [see Fig. 5(a)]. This explains why we do not experience significant numerical problems in calculating the VACF from the GLE in the quadratic lattice.

We conclude that the "problem" of reproducing the exact time correlation functions of a hexagonal harmonic lattice via the GLE with $M^*=\infty$ and the success of the same GLE with $M^*=4$ has a systematic numerical reason which becomes manifest most directly in the mass dependence of $\tilde{\Phi}(\omega)$. From a more physical point of view, we understand this mass dependence as a dependence on the strength of the perturbation induced by the tagged particle on the remaining "bath:" For $M^*=\infty$, the perturbation may be viewed as a static external field to which the "bath" particles must adjust. Given the strong spatial and dynamic correlations characterizing hexagonal lattices (see Sec. IV B and Ref. [33]), it seems then plausible that this perturbation yields a very long lifetime of correlation functions, such as $\Phi^{(M)}(t)$. For $M^* < \infty$, the tagged particle becomes a degree of freedom and thus can "feel" the reaction of the bath. In other words, there is a feedback from the dynamics of the bath particles to that of the tagged particle. As a consequence, the "external field" responds more easily to the bath the smaller M^* becomes. Intuitively, one would therefore anticipate the perturbation to become less and less pronounced, as reflected by the shift (and decreasing magnitude) of the main peak of $\tilde{\Phi}(\omega)$ towards higher frequencies [see Fig. 6(b)]. In our subsequent numerical investigations we therefore fix the mass of the tagged particle in the reference system at a finite, numerically suitable value of M^*.

B. Intermediate temperatures

Increasing the temperature from the very small value of $T^*=10^{-5}$ considered in Sec. IV A the displacements of individual particles from their equilibrium lattice sites become more and more pronounced until the solid finally melts into a dense liquid. Under such conditions, that is, just below or above the melting point, the harmonic approximation of the total potential energy becomes invalid. It then seems particularly interesting to explore the performance of the GLE.

In the following we first estimate the temperature where melting of the present system occurs, focussing exclusively on the hexagonal solid (as explained at the beginning of Sec. IV the quadratic lattice is globally unstable already for temperatures $T^* \gtrsim 10^{-4}$). This estimate is necessary because so far no simulation results for the melting of 2D LJ systems with precisely the same cutoff chosen in the present work exist (for simulations of a slightly different system, see Ref. [34]). We then consider the GLE results for two particularly interesting temperatures below and above the melting point.

1. Estimating the melting point

For three-dimensional systems, a standard way to distinguish fluid and solid phases is to consider the long-time limit of the (system-averaged) mean-squared displacement $f_\Delta(t) = N^{-1}\Sigma_{i=1}^{N}\langle \Delta \mathbf{r}_i^2(t)\rangle$, where $\Delta \mathbf{r}_i(t) = \mathbf{r}_i(t) - \mathbf{r}_i(0)$. In the solid phase this function should approach a constant (corresponding to a vanishing diffusion constant D), contrary to the liquid phase where $f_\Delta(t) \propto Dt$ as $t \to \infty$. In 2D crystals, however, the mean-squared displacement diverges logarithmically with system size [35], indicating a cooperative drift of the particles from their equilibrium sites (indeed, it is well known that formally there is no true long-range order in 2D crystals as signaled by an algebraic decay of the density correlations). On the other hand, it is known (and can be experimentally observed [26,27]) that neighboring particles keep a nearly constant distance from each other even when the system drifts as a whole. Therefore it is sensible to introduce a "local" coordinate system where the particle's displacement is calculated with respect to the positions of its nearest neighbors [36]. These considerations lead to the definition of the so-called dynamic Lindemann parameter [26,27]

$$\gamma_L(t) = \langle [\Delta \mathbf{r}_i(t) - \Delta \mathbf{r}_{i+1}(t)]^2 \rangle / 2r_0^2, \tag{4.3}$$

where r_0 is the mean nearest-neighbor distance [see Eq. (3.3) below]. From Eq. (4.3) it is seen that the function $\gamma_L(t)$ couples the displacements of neighboring particles i and $i+1$. In the crystal, $\gamma_L(t)$ tends to a constant value as t becomes large [36]. On the other hand, in the liquid phase the displacements of the two particles become uncorrelated at long times, such that $\gamma_L(t)$ becomes proportional to the standard mean-squared displacement, $f_\Delta(t)$ [27].

In Fig. 7(a) we plot $\gamma_L(t)$ for the present hexagonal system at various temperatures in the range $0.55 \leqslant T^* \leqslant 1.2$. At $T^*=0.55$ the dynamic Lindemann parameter is bound at large times and this is still the case at $T^*=0.69$. For the latter temperature we find a plateau value of $\gamma_\infty \approx 0.019$, which is typical for a crystalline phase. Indeed, the (universal) "critical" plateau value at which the solid melts is given by $\gamma_\infty^c = 0.033$ [27,36]. At the somewhat higher temperature $T^*=0.72$ and, more visibly, at $T^*=0.76$ we observe from Fig. 7(a) an increasing behavior of $\gamma_L(t)$ at the longest times considered. This increase becomes even more pronounced at the larger temperatures $T^*=0.9$ and $T^*=1.2$. Thus, we estimate the melting temperature T_m^* to be located somewhere in the range $0.69 < T_m^* < 0.72$.

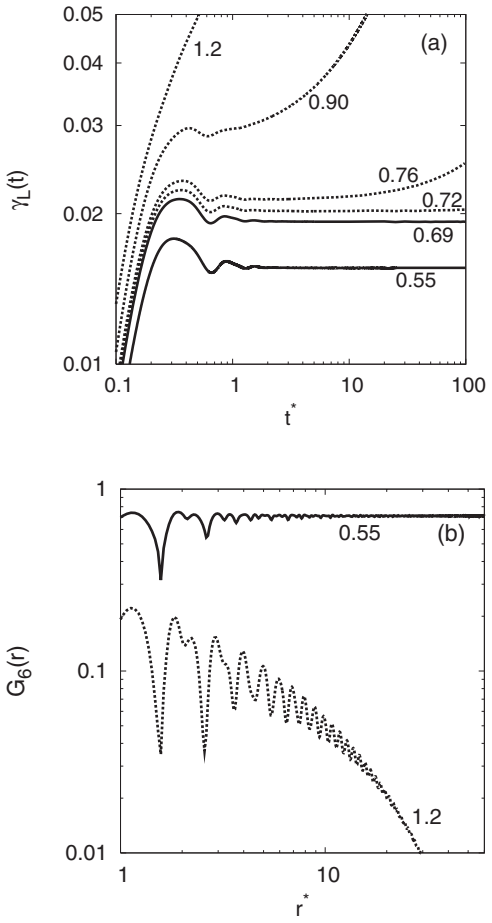

FIG. 7. (a) Dynamic Lindemann parameter $\gamma_L(t)$ at various temperatures T^* indicated by the numbers labeling the curves. Solid and dashed lines are used for solid and liquid phases, respectively. (b) Orientational correlation function $G_6(r)$ at the two temperatures T^* indicated ($r^*=r/\sigma$).

An additional issue in this context is the appearance of a hexatic phase as an intermediate phase between the solid and the isotropic liquid. Such a two-stage melting scenario is predicted by the Kosterlitz-Thouless-Halperin-Nelson-Young (KTHNY) theory [37–40] which was recently confirmed experimentally for 2D systems of paramagnetic colloids [26,27]. There, the topological features (formation of disclination and dislocation pairs) characterizing the two-stage melting can be directly observed by video microscopy. In the present work, however, we are interested in identifying true solid or liquid (rather than hexatic) states since those seem most suitable to investigate the performance of the GLE. To check whether the temperatures identified above fall into the hexatic range we have calculated the (static) bond-orientational correlation function [41]

$$G_6(r) = \langle \Psi_6(\mathbf{r}_1)\Psi_6(\mathbf{r}_2)\rangle, \tag{4.4}$$

where $r=|\mathbf{r}_1-\mathbf{r}_2|$ and $\Psi_6(\mathbf{r}_i)=N_i^{-1}\Sigma_j^{N_i}\exp(6i\theta_{ij})$ is a local bond-angle parameter which is sensitive to the degree of hexagonal ordering around a given particle at $\mathbf{r}_i$ (N_i is the number of nearest neighbors located at $\mathbf{r}_j$, and θ_{ij} is the angle between the vector connecting i and j and the x axis). In a hexagonal solid, $G_6(r)$ decays towards a finite value for large particle separations r, indicating the presence of long-range translational (hexagonal) order in the system. The isotropic liquid, on the other hand, is characterized by an exponential decay of $G_6(r)$ towards zero. Finally, in the hexatic phase $G_6(r)$ decays algebraically signaling quasi-long-range order.

Two results for $G_6(r)$ are plotted in Fig. 7(b) where we have chosen a double-logarithmic representation. At the temperature $T^*=0.55$ the bond order correlation function indicates solidlike behavior in agreement with our dynamical analysis based on the time-dependent Lindemann parameter $\gamma_L(t)$. On the other hand, for $T^*=1.2$ the data presented in Fig. 7(b) reveal that the system is in a truly isotropic liquid state. Indeed, we did not observe indications for a hexatic behavior at the temperatures considered. This is in contrast to a previous simulation study [34] of a slightly different 2D LJ system, where a metastable hexatic phase was found in a very narrow temperature range (and for system sizes much larger than the ones considered in the present work). Whether or not the present system exhibits (meta)stable hexatic phases remains to be explored in a more systematic study with much higher temperature resolution and larger system sizes. Here we concentrate on the temperatures $T^*=0.55$ (solid) and $T^*=1.2$ (liquid) henceforth.

2. Coarse-grained dynamics around the melting point

Numerical results for the velocity and force autocorrelation functions of the tagged particle at $T^*=0.55$ and $T^*=1.2$ are plotted in Fig. 8. We first consider the results corresponding to the solid state [see Fig. 8(a)]. Comparing the original VACF and its reproduction via the GLE we see that the overall agreement is still very good, although the system is far beyond the regime where the harmonic approximation applies. In particular, the GLE correctly describes the original system's temperature [which is proportional to $\Psi_{vv}(t=0)$] as well as the general shape of the VACF and the time interval over which velocity correlations extend. Small quantitative deviations between $\Psi_{vv}(t)$ and $\Psi_{vv}^{(M)}(t)$ occur in that range where the VACF is negative and displays oscillatory behavior. More precise information is revealed by the corresponding force autocorrelation functions plotted in the inset of Fig. 8(a). It is seen that the GLE overestimates the amplitude of the oscillations in the FACF at intermediate times (here, $0.1\lesssim t^*\lesssim 0.6$), indicating that the effective force on the tagged particle itself is not reproduced correctly. This in turn leads to the observed errors in the VACF. On the other hand, short- and long-time behavior of the FACF are again very accurate.

Surprisingly, the GLE still yields reasonable results when we consider the high-density liquid state (characterized by $T^*=1.2$, $\rho^*=0.891$), where the particles are no longer bound to lattice sites neither in the original nor in the reference system. The good quality of the reproduced data is seen when we compare in Fig. 8(b) the original and the GLE data for the VACF (main part) and the FACF (inset). Compared to the solid-state results in Fig. 8(a) the deviations of the reproduced autocorrelation function from their original counterparts are somewhat more pronounced. This concerns in par-

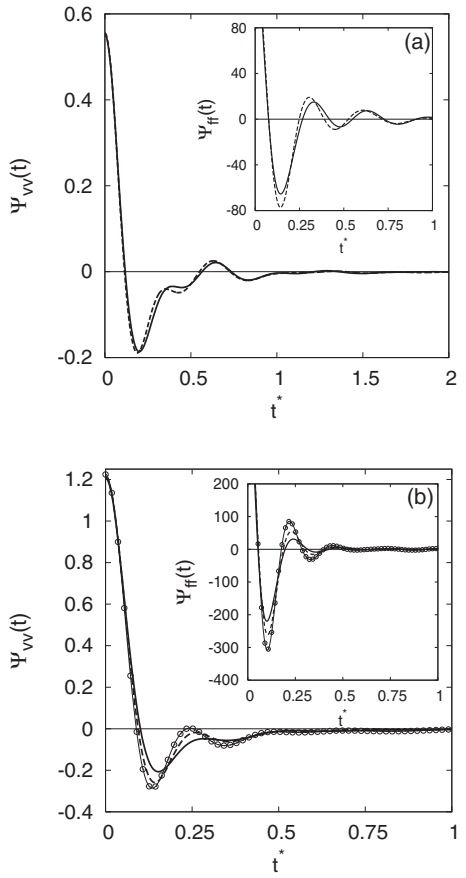

FIG. 8. (a) The functions $\Psi_{vv}(t)$ (solid line) and $\Psi_{vv}^{(M)}(t)$ with $M^*=4$ (dashed line) in the hexagonal solid at $T^*=0.55$. The inset shows the corresponding force autocorrelation functions (in the original system). (b) Same as (a) but in the liquid state at $T^*=1.2$ (and $\rho^*=0.891$). Included are additional results obtained with $M^*=100$ (open circles).

ticular the magnitude of the oscillations in the VACF. These oscillations reflect backscattering effects which are overestimated the more the larger M^* becomes. However, at a qualitative level, the GLE still reproduces the main features of the correlation functions. This is a remarkable result which may be due to the fact that the local positional order at the high density considered is already very similar to what one finds in the hexagonal solid stabilized at lower temperatures. From that point of view one would expect less accurate results at lower densities. We will revisit this issue in the subsequent Sec. IV C.

Here it is interesting to briefly consider the role of the mass M chosen for the tagged particle in the reference system for the predictions of the GLE. We recall that in a perfect harmonic system the value of M is arbitrary [20] (despite from the practical, that is, numerical considerations discussed in Sec. IV A). In an anharmonic system such as a liquid, however, perfect agreement [between, say, $\Psi_{vv}(t)$ and $\Psi_{vv}^{(M)}(t)$] should only occur for the trivial choice $M=m_0$ (i.e., $M^*=1$) for which the integral term in Eq. (2.16) vanishes and the reference system reduces to the original one. From that point of view, we expect the deviations to increase with increasing dimensionless mass M^*. That this is indeed true can be seen from the additional data plotted in Fig. 8(b), which refer to $M^*=100$. The differences between the cases $M^*=100$ and $M^*=4$ are particularly pronounced in the FACF (inset). Indeed, it seems that increasing the mass ratio has a similar effect than increasing the temperature, that is an enhancement of the amplitude of the oscillations. On the other hand, upon further increase of the mass ratio the effective force- and velocity-autocorrelation functions rapidly converge to limiting functions. For instance, the autocorrelation functions obtained with $M^*=10^4$ are nearly indistinguishable from those at $M^*=100$, indicating that the precise value of M is not very important in this range. This is also confirmed by the behavior of the corresponding power spectra (not shown) of the kernel $\Phi^{(M)}(t)$ determining the integral in the GLE (2.16).

C. Liquids at lower densities

Given the very good performance of the GLE in the melt ($\rho^*=0.891$) it is interesting to explore the influence of particle density within the liquid state. Indeed, the lower the density, the less we expect the local positional structure in the system to resemble that of a harmonic solid for which the GLE was constructed originally. As an example we consider the density $\rho^*=0.6$. Results for the VACF and the FACF of the tagged particle and the corresponding reproduced data are plotted in Fig. 9(a), where we have chosen $M^*=4$ and $M^*=100$. Considering first the original data we see that, as expected, the VACF has a simpler structure compared to the high-density case [see Fig. 8(b)]. Whereas the latter reveals a pronounced cage effect (see the two negative minima), the VACF at $\rho^*=0.6$ decays monotonically and smoothly to zero. Still, the GLE is not capable of fully reproducing these data, with the deviations becoming more pronounced the larger M^* is. This is consistent with the observations made at high densities (see Sec. IV B). In particular, for $M^*=100$ we observe from Fig. 9(a) that the reproduced VACF has oscillations absent in the original data. Corresponding deviations are also seen in the FACF plotted in the inset of Fig. 9(a).

A natural measure to quantify such deviations in the liquid phase would be to calculate the diffusion constant via the (Green-Kubo) integral of the VACF. However, it is well known that in 2D fluids at moderate density the VACF possesses a long-time tail ($\sim t^{-1}$) [42] due to hydrodynamic backflow effects [12], and a similar behavior is observed in the present numerical data. Thus, it becomes problematic to evaluate the Green-Kubo integral numerically. As an alternative, we integrate the squared difference between the VACF and its reproduction, yielding the time-dependent function

$$\Gamma(t) = \int_0^t [\Psi_{vv}(t') - \Psi_{vv}^{(M)}(t')]^2 dt'. \tag{4.5}$$

Results for $\Gamma(t)$ at $\rho^*=0.6$ are given in Fig. 9(b), where we have included corresponding data obtained at the high density $\rho^*=0.891$. It is seen that substantial contributions to $\Gamma(t)$ occur at times $t^* \lesssim 0.5$ as indicated by the plateaus reached by $\Gamma(t)$ at later times. The other main conclusion is that, for fixed value of M^*, the absolute deviation (as given by the

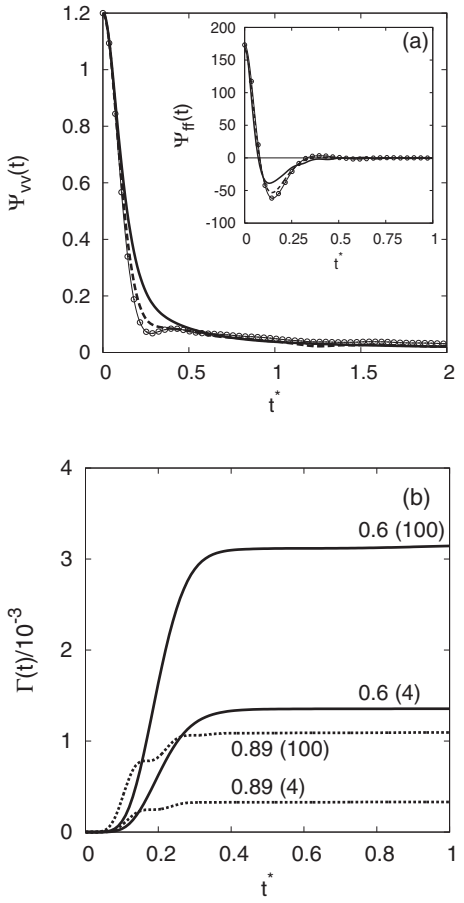

FIG. 9. (a) The functions $\Psi_{vv}(t)$ (solid lines) and $\Psi_{vv}^{(M)}(t)$ with $M^*=4$ (dashed lines) and $M^*=100$ (open circles) at $\rho^*=0.6$ and $T^*=1.2$. The inset shows the corresponding FACFs. (b) The functions $\Gamma(t)$ for the two densities $\rho^*=0.6$ (solid lines) and $\rho^*=0.891$ (dashed lines), with the reference system being characterized by $M^*=4$ and 100. These values are indicated at the curves with the notation ρ^* (M^*).

plateau value) indeed increases significantly upon decrease of ρ^*. This confirms our expectation that the GLE generally becomes less accurate when the local structure becomes increasingly more liquidlike.

V. CONCLUSIONS

The main goal of the present paper is to explore the suitability of a generalized Langevin equation, which is exact in harmonic solids, to describe the single-particle dynamics in "anharmonic" situations such as high-temperature solids and liquids. To this end we have performed MD simulations of a two-dimensional model system and a corresponding reference system. The latter is needed to compute the key ingredient of the GLE, that is, the random force and its correlations determining the kernel. Our main finding is that the GLE works surprisingly well even if the structure of the actual system is very different from that of a harmonic solid. As a side product, the present simulations also illustrate some specific physical properties of the 2D LJ system considered here. In this context, the most prominent features are the long lifetime of correlations in the low-temperature hexagonal phase, and the presence of collective displacements close to the melting point which motivates the use of a modified dynamic Lindemann parameter.

The good performance of the GLE at finite temperatures is particularly remarkable in view of the fact that the mass of the tagged particle in our original system m_0 was set equal to the mass m characterizing the remaining bath particles. This choice corresponds, in a way, to a "worst-case" situation since the resulting kernel $\Phi^{(M)}(t)$ [which is determined by the motion of the bath particles] then decays on the same time scale as dynamic correlations (e.g., the VACF) of the tagged particle. Indeed, one would expect even better performance of the GLE if $m_0 \gg m$, corresponding to the classical situation of a heavy colloidal particle in a solvent. In the latter case, $\Phi^{(M)}(t)$ should decay on a time scale much shorter than the time scale governing fluctuations in the heavy particle's momentum. In other words, the two time scales should separate, with the consequence that the detailed structure of $\Phi^{(M)}(t)$ becomes irrelevant for the resulting integral appearing in the GLE (which in turn yields a much higher tolerance for the actual computation of the kernel). Thus, a detailed investigation of the influence of the mass ratio m_0/m on the performance of the GLE would be worthwhile. Another interesting topic concerns the influence of additional conservative forces resulting from the presence of several tagged particles. The original GLE proposed by Deutch and Silbey can be easily generalized to this situation [19].

Of course, given that the original idea behind using GLE's (and other coarse-graining concepts) is to reduce computational burden, investigations of the present type which rely on parallel simulations of two many-particle systems (the original and the reference one) appear rather elaborate. From that point of view, it is encouraging to see that (according to our results in Sec. IV A) some main features of the kernel $\Phi^{(M)}(t)$ and its power spectrum (such as the mass dependence) may be inferred from simple concepts such as a harmonic oscillator. This finding might serve as a guide for a future development of simple models of the kernel. Such an approach would be similar in spirit to basic concepts of mode-coupling theory [12]. Another approach to modeling the kernel has been suggested in numerous papers by Adelman and co-workers (see Ref. [43] for a comprehensive review). Here one maps the GLE onto a one-dimensional harmonic chain of pseudoparticles immersed in a heat bath where the heat bath is modelled by a hierarchy of time correlation functions. The hierarchy is then truncated at some level by making a Markovian approximation. The applicability of such concepts on the problems discussed in the present work is currently under investigation.

ACKNOWLEDGMENTS

We gratefully acknowledge financial support from the Deutsche Forschungsgemeinschaft through the Sonderforschungsbereich 448 "Mesoscopically structured composites" (Projects No. B6 and No. B11). We would also like to thank Professor M. Berkowitz for bringing to our attention the work of Adelman (Ref. [43]).

APPENDIX A: DERIVATION OF THE GLE

1. Derivation of the operator identity (2.6)

In this appendix we first derive an analog of Eq. (2.6) [44], which is more general since it does not rely [contrary to Eq. (2.6)] on the assumption that the Liouville operators are independent of time. We then specialize to the case considered in the present work.

We depart from the Liouville equation for an arbitrary operator $\mathcal{U}(t,t_0)$,

$$\dot{\mathcal{U}}(t,t_0) = i\mathcal{L}(t)\mathcal{U}(t,t_0), \tag{A1}$$

in which the Liouville operator $\mathcal{L}(t)$ may be explicitly time dependent. We supplement Eq. (A1) by the initial condition $\mathcal{U}(t_0,t_0)=1$. Splitting $\mathcal{L}(t)$ according to Eq. (2.4), and introducing a second operator through $\dot{\mathcal{U}}^B(t,t_0) = i\mathcal{L}^B(t)\mathcal{U}^B(t,t_0)$ [with the initial condition $\mathcal{U}_B(t_0,t_0)=1$] one may prove (see below) the exact relation

$$\mathcal{U}(t,t_0) = \mathcal{U}_B(t,t_0) + \int_{t_0}^{t} \mathcal{U}(t,t')i\mathcal{L}^{(0)}(t')\mathcal{U}_B(t',t_0)dt' \equiv \mathcal{X}(t,t_0). \tag{A2}$$

To verify Eq. (A2) we note that two time-dependent operators are identical if they have the same time derivative and coincide at $t=t_0$. The latter property immediately follows from the fact that the integral on the right side of Eq. (A2) disappears at $t=t_0$ and that $\mathcal{U}(t_0,t_0)=\mathcal{U}_B(t_0,t_0)=1$.

Thus, we consider the time derivative of Eq. (A2), where the left side simply follows from the Liouville equation (A1). The derivative of the right side becomes

$$\begin{aligned}\dot{\mathcal{X}}(t,t_0) &= \dot{\mathcal{U}}_B(t,t_0) + \underbrace{\mathcal{U}(t,t)}_{=1} i\mathcal{L}^{(0)}(t)\mathcal{U}_B(t,t_0) \\ &\quad + \int_{t_0}^{t} \dot{\mathcal{U}}(t,t')\mathcal{L}^{(0)}(t')\mathcal{U}_B(t',t_0)dt' \\ &= i\mathcal{L}^{(B)}(t)\mathcal{U}_B(t,t_0) + i\mathcal{L}^{(0)}(t)\mathcal{U}_B(t,t_0) \\ &\quad + i\mathcal{L}(t)\int_{t_0}^{t} \mathcal{U}(t,t')\mathcal{L}^{(0)}(t')\mathcal{U}_B(t',t_0)dt',\end{aligned} \tag{A3}$$

where we have used the Liouville equation for $\mathcal{U}$ [see Eq. (A1)] and the analogous one for $\mathcal{U}_B$. Summarizing the first two terms on the far right side of Eq. (A3) and comparing with the definition of $\mathcal{X}$ given in Eq. (A2), we find

$$\dot{\mathcal{X}}(t,t_0) = i\mathcal{L}(t)\mathcal{X}(t,t_0). \tag{A4}$$

Thus, $\mathcal{X}$ satisfies the same differential equation as $\mathcal{U}$ [see Eq. (A1)], which completes our proof of Eq. (A2).

In the context of this work the operators $\mathcal{L}$, $\mathcal{L}^{(B)}$, and $\mathcal{L}^{(0)}$ exhibit no explicit time dependence. We can then formally integrate the Liouville equation [see Eq. (A1)] to obtain $\mathcal{U}(t,t_0)=\exp[i\mathcal{L}(t-t_0)]$ and, analogously, $\mathcal{U}^B(t,t_0) = \exp[i\mathcal{L}^B(t-t_0)]$. Replacing the latter expressions into Eq. (A2) and setting $t_0=0$ gives Eq. (2.6).

2. Derivation of Eq. (2.11)

We start by considering the first member of Eq. (2.11), which implies that $\mathcal{P}i\mathcal{L}^{(B)}\mathbf{F}_0^+(t)=0$. Since, according to Eq. (2.9), $\mathbf{F}_0^+(t)=\exp(i\mathcal{L}^{(B)}t)\mathbf{F}_0(0)$, and since the operators $\mathcal{L}^{(B)}$ and $\exp(i\mathcal{L}^{(B)}t)$ commute with one another, it is sufficient to show that $\mathcal{P}i\mathcal{L}^{(B)}=0$. To see this we use the explicit expression for the action of $\mathcal{P}$ given in Eq. (2.10) and the definition of $\mathcal{L}^{(B)}$ [see Eq. (2.5b)], yielding

$$\begin{aligned}\mathcal{P}i\mathcal{L}^{(B)} &= \frac{1}{Q'(\mathbf{r}_0)}\prod_{i=1}^{N}\int d\mathbf{p}_i \int d\mathbf{r}_i i\mathcal{L}^{(B)} \exp(-\beta H') \\ &= -\frac{\beta}{Q'(\mathbf{r}_0)}\prod_{i=1}^{N}\int d\mathbf{p}_i \int d\mathbf{r}_i \sum_{j=1}^{N}\left(\frac{\mathbf{p}_j}{m}\frac{\partial H'}{\partial \mathbf{r}_j} + \mathbf{F}_j\frac{\partial H'}{\partial \mathbf{p}_j}\right) \\ &\quad \times\exp(-\beta H') \\ &= -\frac{\beta}{Q'(\mathbf{r}_0)}\prod_{i=1}^{N}\int d\mathbf{p}_i \int d\mathbf{r}_i \sum_{j=1}^{N}\left(\frac{\mathbf{p}_j}{m}\frac{\partial U}{\partial \mathbf{r}_j} + \mathbf{F}_j\frac{\mathbf{p}_j}{m}\right) \\ &\quad \times\exp(-\beta H') = 0.\end{aligned} \tag{A5}$$

In obtaining the last line we have used the definition of the Hamiltonian H' [see Eq. (2.1)]. The last zero then simply follows from the fact that $\partial U/\partial \mathbf{r}_j = -\mathbf{F}_j$ so that the expression in brackets vanishes for each j independently.

To verify the second member of Eq. (2.11), consider [using Eq. (2.5a)]

$$\begin{aligned}\mathcal{P}i\mathcal{L}^{(0)}\mathbf{F}_0^+(t) &= \frac{1}{Q'(\mathbf{r}_0)}\prod_{i=1}^{N}\int d\mathbf{p}_i \int d\mathbf{r}_i \\ &\quad \times\left(\frac{\mathbf{p}_0}{m_0}\frac{\partial}{\partial \mathbf{r}_0} + \mathbf{F}_0\frac{\partial}{\partial \mathbf{p}_0}\right)\mathbf{F}_0^+(t)\exp(-\beta H') \\ &= \frac{\mathbf{p}_0}{m_0}\left\langle\frac{\partial \mathbf{F}_0^+(t)}{\partial \mathbf{r}_0}\right\rangle + \frac{\partial}{\partial \mathbf{p}_0}\langle\mathbf{F}_0(0)\cdot\mathbf{F}_0^+(t)\rangle.\end{aligned} \tag{A6}$$

In writing the last term we have used that the force $\mathbf{F}_0$ is conservative and therefore independent of $\mathbf{p}_0$. Moreover, since we are performing an equilibrium average, $\mathbf{F}_0$ appears as a time-independent quantity which we can therefore set equal to $\mathbf{F}_0(0)$.

To evaluate the first term on the far right side we make use of the fact that the time average of the random force vanishes, that is, $\langle\mathbf{F}_0^+(t)\rangle=0$. As a consequence, a spatial derivative of this average vanishes as well. Combining this fact with the product rule, we find

$$\begin{aligned}\frac{\partial}{\partial \mathbf{r}_0}\langle\mathbf{F}_0^+(t)\rangle &= 0 \\ &= \frac{\partial}{\partial \mathbf{r}_0}\left(\frac{1}{Q'(\mathbf{r}_0)}\prod_{i=1}^{N}\int d\mathbf{p}_i \int d\mathbf{r}_i \mathbf{F}_0^+(t)\exp(-\beta H')\right) \\ &= \left\langle\frac{\partial \mathbf{F}_0^+(t)}{\partial \mathbf{r}_0}\right\rangle + \beta\langle\mathbf{F}_0(0)\cdot\mathbf{F}_0^+(t)\rangle.\end{aligned} \tag{A7}$$

Solving Eq. (A7) with respect to $\langle\partial\mathbf{F}_0^+(t)/\partial\mathbf{r}_0\rangle$, and inserting the result into Eq. (A6), we obtain

$$\mathcal{P}[i\mathcal{L}^{(0)}\mathbf{F}_0^+(t)] = \left(\frac{\partial}{\partial \mathbf{p}_0} - \frac{\beta \mathbf{p}_0}{m_0}\right)\langle \mathbf{F}_0(0)\cdot\mathbf{F}_0^+(t)\rangle$$
$$= \left(\frac{\partial}{\partial \mathbf{p}_0} - \frac{\beta \mathbf{p}_0}{m_0}\right)\langle \mathbf{F}_0^+(0)\cdot\mathbf{F}_0^+(t)\rangle, \quad \text{(A8)}$$

where the last line follows from the fact that, at $t=0$, the forces $\mathbf{F}_0$ and $\mathbf{F}_0^+$ becomes identical [see Eq. (2.9)].

APPENDIX B: SIMULATION DETAILS

In our MD simulations the equations of motion were integrated using the velocity-Verlet algorithm [45] with a time step of $\Delta t^* = 10^{-3}$ (the reduced time is defined as $t^* = t\sqrt{\varepsilon/m\sigma^2}$). In order to reduce finite size effects we apply periodic boundary conditions in x and y directions in all of our simulations. However, at very low temperatures this standard procedure alone leads to artifacts in the time correlation functions such as the force autocorrelation function defined in Eq. (3.5). For a finite crystalline system (at low temperatures) these functions display recurring patterns whose recurrence frequency decreases with increasing system size. We can interpret these recurring patterns as sound waves propagating through the system. When reaching the boundary of the simulation cell these waves reenter the cell from the opposite side due to the periodic boundary conditions. To circumvent this problem we supplement these conventional boundary conditions by so-called stochastic boundary conditions [46]. Within this framework those bath particles which are "far away" (in practice, $\sim 25\sigma$) from the tagged particle at the center of the simulation cell, "feel" nonconservative forces $\mathbf{F}_i^{\mathrm{nc}}$ in addition to the conservative (pair) forces resulting from the neighboring particles. These forces are of Brownian type, but chosen in such a way that the total momentum of the entire system is conserved in each time step (contrary to conventional Brownian dynamics). More specifically, we set $\mathbf{F}_i^{\mathrm{nc}} = -\gamma(\mathbf{v}_i - \Sigma_j \mathbf{v}_j) + \alpha\tilde{\chi}_i/\sqrt{\Delta t}$ where γ is the friction coefficient and α is the amplitude of the random force. In $\tilde{\chi}_i = \chi_i - \Sigma_j \chi_j$ the components of the vector χ_i are uniformly distributed random numbers sampled from the interval $[-1;1]$. The presence of the frictional and random forces enables those bath particles, that are located close to the boundaries of the simulation cell to dissipate energy from an incoming sound wave. In this way, the sound waves are effectively damped out. In order to model a canonical system with fixed temperature T, the parameters γ and α were chosen according to the fluctuation-dissipation theorem, that is, $k_B T = \alpha^2/2\gamma$.

Clearly, one would like to avoid any influence of the nonconservative forces acting at the boundaries on the dynamics of the tagged particle in the cell center. This is achieved by using sufficiently large system sizes, i.e., we set the side lengths of the simulation cell equal to 40 times the side lengths l_x, l_y of subcells depicted in Fig. 1. Moreover, a small amplitude γ of the frictional forces is chosen.

Upon increasing the temperature towards the melting point the sound-wave problem described above essentially disappears. The corresponding MD simulations (see Sec. IV B) are therefore carried out without stochastic boundary conditions. The same holds for the MD simulations within the liquid state described in Sec. IV C.

All simulations begin with an equilibration period of about 10^5 time steps, after which we start to collect averages of the dynamical quantities of interest (see Sec. III). For the original system, these are the correlation functions $\Psi_{ff}(t)$ and $\Psi_{vv}(t)$ defined in Eqs. (3.5) and (3.4), respectively. Since these autocorrelation functions involve only one (the "tagged") particle, averaging over many time origins is required to obtain sufficient statistics. We have used 2×10^5 samples corresponding to a total production period of 10^8 time steps. Similar effort is required for the reference system where we calculate, for given mass M, the autocorrelation function $\Phi^{(M)}(t) = \langle \mathbf{F}_0^{(M)}(0)\mathbf{F}_0^{(M)}(t)\rangle$. Finally, we also store the function $\mathbf{F}_0^{(M)}(t)$ which is the second key ingredient for the GLE [see Eq. (2.16)].

[1] *Novel Methods in Soft Matter Simulations*, edited by M. Karttunen, I. Vattulainen, and A. Lukkarinen, *Lecture Notes in Physics* No. 640 (Springer, Berlin, 2004).
[2] F. Müller-Plathe, Soft Mater. **1**, 1 (2003).
[3] A. van den Noort, W. K. den Otter, and W. J. Briels, Europhys. Lett. **80**, 28003 (2007).
[4] P. J. Hoogerbrugge and J. M. V. A. Koelman, Europhys. Lett. **19**, 155 (1992); J. M. V. A. Koelman and P. J. Hoogerbrugge, *ibid.* **21**, 363 (1993).
[5] R. D. Groot and P. B. Warren, J. Chem. Phys. **107**, 4423 (1997).
[6] C. N. Likos, Phys. Rep. **348**, 267 (2001).
[7] S. H. L. Klapp, D. J. Diestler, and M. Schoen, J. Phys.: Condens. Matter **16**, 7331 (2004).
[8] H. Bock, K. E. Gubbins, and S. H. L. Klapp, Phys. Rev. Lett. **98**, 267801 (2007).
[9] S. H. L. Klapp, J. R. Silbermann, and M. Schoen, Mol. Phys. **105**, 1039 (2007).
[10] H. Mori, Prog. Theor. Phys. **33**, 423 (1965).
[11] R. Zwanzig, Phys. Rev. **124**, 983 (1961).
[12] J. P. Hansen and I. R. McDonald, *Theory of Simple Liquids*, 3rd. ed. (Academic, London, 2006).
[13] R. L. C. Akkermans and W. J. Briels, J. Chem. Phys. **113**, 6409 (2000).
[14] O. F. Lange and H. Grubmüller, J. Chem. Phys. **124**, 214903 (2006).
[15] M. Stepanova, Phys. Rev. E **76**, 051918 (2007).
[16] S. Izvekov and G. A. Voth, J. Chem. Phys. **125**, 151101 (2006).
[17] D. Cubero and S. N. Yaliraki, J. Chem. Phys. **122**, 034108 (2005).
[18] T. Kinjo and S. A. Hyodo, Phys. Rev. E **75**, 051109 (2007).
[19] J. M. Deutch and R. Silbey, Phys. Rev. A **3**, 2049 (1971).
[20] K. Wada and J. Hori, Prog. Theor. Phys. **49**, 129 (1973).

[21] M. Kröger, Soft Matter **4**, 18 (2008).
[22] M. Kröger, Phys. Rep. **390**, 453 (2004).
[23] P. Espanol, Phys. Rev. E **53**, 1572 (1996).
[24] C. Hijon, M. Serrano, and P. Espanol, J. Chem. Phys. **125**, 204101 (2006).
[25] P. Keim, G. Maret, U. Herz, and H. H. von Grünberg, Phys. Rev. Lett. **92**, 215504 (2004).
[26] K. Zahn, R. Lenke, and G. Maret, Phys. Rev. Lett. **82**, 2721 (1999).
[27] K. Zahn and G. Maret, Phys. Rev. Lett. **85**, 3656 (2000).
[28] M. J. Vlot and J. P. van der Eerden, J. Chem. Phys. **109**, 6043 (1998).
[29] B. J. Alder and T. E. Wainwright, Phys. Rev. **127**, 359 (1962).
[30] W. G. Hoover and S. Hess, Physica A **267**, 98 (1999).
[31] D. A. McQuarrie, *Statistical Mechanics* (Harper & Row, New York, 1976).
[32] B. J. Berne and G. D. Harpe, in *Advanced Chemical Physics*, edited by I. Prigogine and S. A. Rice (Interscience Publishers, New York, 1970), Vol. XVII.
[33] J. R. Silbermann, Ph.D. thesis, Technische Universität Berlin, Berlin, 2008.
[34] K. Chen, T. Kaplan, and M. Mostoller, Phys. Rev. Lett. **74**, 4019 (1995).
[35] N. D. Mermin, Phys. Rev. **176**, 250 (1968).
[36] V. M. Bedanov and G. V. Gadiyak, Phys. Lett. **109A**, 289 (1985).
[37] J. M. Kosterlitz and D. J. Thouless, J. Phys. C **6**, 1181 (1973).
[38] B. I. Halperin and D. R. Nelson, Phys. Rev. Lett. **41**, 121 (1978).
[39] D. R. Nelson and B. I. Halperin, Phys. Rev. B **19**, 2457 (1979).
[40] A. P. Young, Phys. Rev. B **19**, 1855 (1979).
[41] K. J. Strandburg, Rev. Mod. Phys. **60**, 161 (1988).
[42] B. J. Alder and T. E. Wainwright, Phys. Rev. A **1**, 18 (1970).
[43] S. A. Adelman, Adv. Chem. Phys. **40**, 143 (1980).
[44] E. Fick and G. Sauermann, *Quantenstatistik Dynamischer Prozesse* (Verlag Harry Deutsch, Frankfurt am Main, 1983), Bd. I.
[45] M. P. Allen and D. J. Tildesley, *Computer Simulation of Liquids* (Academic, London, 1987).
[46] M. Berkowitz, and J. A. McCammon, Chem. Phys. Lett. **90**, 215 (1982).